

Article

# Effect of ECAP Die Angle on Mechanical Properties and Biocompatibility of SS316L

Dayangku Noorfazidah Awang Sh'ri <sup>1,\*</sup>, Zahiruddeen Salam Zahari <sup>1</sup> and Akiko Yamamoto <sup>2</sup>

<sup>1</sup> Department of Mechanical Engineering, Engineering Collage, Universiti Malaysia Pahang, 26300 Gambang, Pahang, Malaysia; zahirsalam95@gmail.com

<sup>2</sup> Research Center for Functional Materials, National Institute for Materials Science, Namiki 1-1, Tsukuba 305-0044, Ibaraki, Japan; yamamoto.akiko@nims.go.jp

\* Correspondence: noorfazidah@ump.edu.my; Tel.: +81-609-424-6311

**Abstract:** In this study, ultrafine grain (UFG) SS316L was produced using an equal channel angular pressing (ECAP) process at two different die angles namely 120° and 126°. The effect of different die angles on mechanical, corrosion, and surface properties were thoroughly investigated. Furthermore, the subsequent effect on the cytotoxicity of SS316L was investigated. The microstructure observation shows ECAP processing has produced an elongated, finer grain size at 120° than 126°. The ECAP processing also increases the hardness of SS316L. There is no change in wettability and surface roughness observed. However, the electrochemical measurement reveals that ECAP processing improves the corrosion resistance of SS316L. The cytocompatibility of ECAPed SS316L was evaluated by both a direct and an extract methods, finding the contribution of grain refinement by ECAP processing.

**Keywords:** equal channel angular pressing; stainless steel 316L; die angle; severe plastic deformation



**Citation:** Awang Sh'ri, D.N.; Zahari, Z.S.; Yamamoto, A. Effect of ECAP Die Angle on Mechanical Properties and Biocompatibility of SS316L. *Metals* **2021**, *11*, 1513. <https://doi.org/10.3390/met11101513>

Academic Editor: Massimo Pellizzari

Received: 9 September 2021

Accepted: 22 September 2021

Published: 24 September 2021

**Publisher's Note:** MDPI stays neutral with regard to jurisdictional claims in published maps and institutional affiliations.



**Copyright:** © 2021 by the authors. Licensee MDPI, Basel, Switzerland. This article is an open access article distributed under the terms and conditions of the Creative Commons Attribution (CC BY) license (<https://creativecommons.org/licenses/by/4.0/>).

## 1. Introduction

Severe plastic deformation (SPD) is a metalworking process that produces high defect density and consistent ultrafine grain structure or crystalline with nano structure by combining enormous strains with a characteristic complicated stress state or high shear in the specimen. The SPD technique was developed in the 1930s and started to gain interest in the past few decades. The SPD processes include equal channel angular pressing (ECAP), high pressure torsion (HPT), accumulative roll bonding (ARB), and multidirectional forging (MDF). Furthermore, many novel methods have been done to improve the technical capabilities of the existing SPD methods including tubular channel angular pressing [1], vortex extrusion [2] and sideways extrusion [3,4]. Equal channel angular pressing (ECAP) remains one of the popular severe plastic deformation processes first introduced in the 1980s by Segal [5,6], and later improved by Ruslan Valiev [7–9]. In the ECAP process, the sample will be pressed through an angular channel with the same cross-sectional area under extremely high shear strain. By initiating high plastic strain into the materials, ECAP improves the mechanical properties of the materials without changing their cross-sectional area [10]. The process produces superior mechanical properties on the materials while maintaining their shape and dimension [11]. Deformation of the ECAPed samples during a single pass is related to the parameters of ECAP processing, such as the temperature, the channel angle, and the outer radius angle. The channel angle of the common ECAP die is 90°, which exerts very large single-pass shearing deformation. However, at a die angle of 90°, a high processing temperature is needed to avoid the fracture of samples. Thus, increasing the die angle allows the shear deformation to avoid specimen fracture, resulting in dynamic recrystallization [12]. Furthermore, a higher die angle will decrease the pressing force required [13]. To ease the sample extrusion required during ECAP especially at room temperature, many researchers have adopted higher die angle even though it resulted in smaller equivalent strain [14–16].

Stainless steel (SS) 316L is primarily used in biomedical applications for implantable devices due to its excellent corrosion resistance, high oxidation resistance, and good formability [17]. This steel contains significantly more nickel than conventional austenitic steel, ensuring a fully austenitic state [18]. However, the high nickel content is the primary impediment to using steel in biomedical applications, as nickel and its compounds are potent allergens. The corrosion resistance of the SS is attributed to the presence of protective passive film which stability is largely influenced by the Cr content of the alloy. However, the passive film on SS is susceptible to localized breakdown (pitting corrosion) [19]. It has been found that nanocrystalline grain size has been shown to improve the pitting resistance and passivation behaviour of the steels [20]. Thus, by applying the ECAP process on the stainless steel, we may alter the grain structure and consequently improved the corrosion behaviour. In this present study, we aimed to manufacture ultrafine grained SS316L at two different die angles namely  $120^\circ$  and  $126^\circ$ . Consequently, we systematically investigated the effect of ECAP die angle on the mechanical, electrochemical, and surface properties of SS316 and their influence on the cytocompatibility of SS316L.

## 2. Materials and Methods

### 2.1. Mechanical and Microstructure Properties

Commercial heat-treated SS316L with 10 mm diameter and 15 cm length was used as the sample in this work. Two sets of ECAP dies with internal die angles of  $120^\circ$  and  $126^\circ$ , respectively, were used as shown in Figure 1. The channel diameter of the die was 260 mm with a channel diameter of 10 mm. The samples were pressed at room temperature for one pass for each of the die at a pressure of 80 bar by using a hydraulic pressure machine. Molybdenum disulphide ( $\text{MoS}_2$ ) was used for this process to reduce the friction between the sample surface and the channel surface.

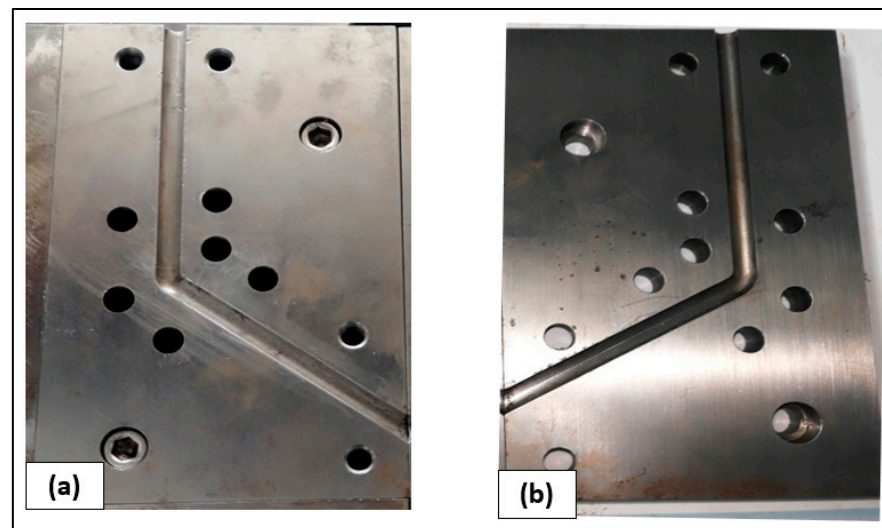


**Figure 1.** Insert of ECAP die with internal die angle of (a)  $120^\circ$  and (b)  $126^\circ$ .

For microstructure analysis, a metallurgical microscope (Olympus BX53, Melville, NY, USA) was used. The image of the microstructure appeared after being etched using Carpenters stainless steel etch. Only one of each condition was tested. Toupview software (Hangzhou ToupTek Photonics Co., Ltd., Hangzhou, China) was used to further analysis of grain size and particles area.

The hardness of ECAPed specimens was investigated using Vickers hardness machine (Wilson Tukon 1202, Lake Bluff, IL, USA). The specimens were subjected to a load of 100 gf for 10 s. The test was carried out in a grid of seven points horizontally and three points vertically to check the hardness distribution across the samples (Figure 2).

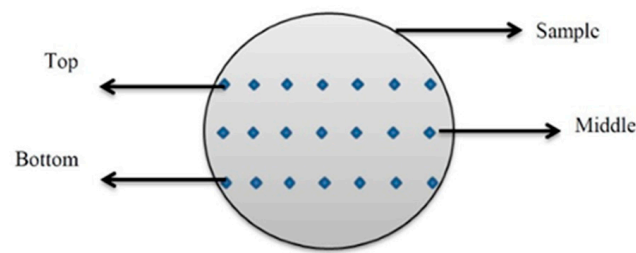


**Figure 2.** Hardness test points.

## 2.2. Electrochemical Test

SS316L specimens were polished by SiC papers upto UF-1200 (6.5  $\mu\text{m}$ ), and sterilized by ethylene oxide gas prior to the electrochemical test. The test was performed using a typical three electrode system consisting of a platinum wire as a counter electrode, a saturated Ag/AgCl (3 M NaCl) electrode as a reference electrode, and an SS316L sample (exposed area of 0.264  $\text{cm}^2$ ) as a working electrode. The electrodes setup was connected to a potentiostat (VersaSTAT 4, Princeton Applied Research, AMETEK, Oak Ridge, TN, USA). A 5 mL portion of an electrolyte was poured into the electrochemical test chamber, and placed in an incubator at a certain temperature for approximately 2 h to stabilize the the open-circuit potential (OCP). Then, potentiodynamic (PD) measurement was performed at a scanning rate of 0.16 mV/s with the potential range from  $-0.25$  V vs. open circuit potential (OCP) to the potential giving the current over 1  $\text{mA}/\text{cm}^2$ . Parameters such as corrosion potential ( $E_{\text{corr}}$ ) and corrosion current density ( $I_{\text{corr}}$ ) were decided from polarization curves by the Tafel method using VersaStudio software (Princeton Applied Research, AMETEK, Oak Ridge, TN, USA). Testing conditions were as follows:

- (1) In 0.9% NaCl at 37  $^{\circ}\text{C}$  with  $\text{N}_2$  flow at 100 mL/min,
- (2) In a cell culture medium at 37  $^{\circ}\text{C}$  under an atmosphere of 5%  $\text{CO}_2$  in humidified air.

As the cell culture medium, Eagle's minimum essential medium supplemented with 10% newborn calf serum (E-MEM + 10%NCS) was employed with pre-conditioning overnight at the same condition to the test. At least three samples were tested for each condition.

## 2.3. Cytotoxicity Test

Cytotoxicity test was performed following ISO10993-5 (direct method and extract method). Murine fibroblast L929 (NCTC Clone 929, purchased from Dainippon Pharmaceutical Co. Ltd., Osaka, Japan) was employed. All surfaces of SS316L disc samples 6~9 mm in diameter and 4~5 mm in thickness were polished by SiC paper up to UF-1200 (6.5  $\mu\text{m}$ ). Then, polished samples were sterilized by ethylene oxide gas prior to the test.

For the direct method, disc samples were placed in the bottom of 24-well microplate and then, 100 cells for L929 were inoculated with 1mL of E-MEM supplemented with 10% fetal bovine serum (E-MEM + 10%FBS). Control well is prepared as the well without a sample. After 7d of incubation at 37  $^{\circ}\text{C}$  in an atmosphere of 5%  $\text{CO}_2$  in humidified air, cells are fixed with a 25% glutaraldehyde solution and stained with a 10% Giemsa staining solution. The number of colonies formed on the sample surface or the bottom of the control well was counted to calculate the relative plating efficiency (RPE) as follows:

$$\text{RPE (\%)} = \{(N_{\text{sample}}/A_{\text{sample}})/(N_{\text{control}}/A_{\text{control}})\} \times 100$$

where  $N_{\text{sample}}$  and  $N_{\text{control}}$  indicate the average number of colonies on the sample surface and on the bottom of the control well, respectively.  $A_{\text{sample}}$  and  $A_{\text{control}}$  indicate the sample top surface area and the bottom area of the control well, respectively.

For the extract method, five samples were immersed into E-MEM + 10%FBS at 37  $^{\circ}\text{C}$  in an atmosphere of 5%  $\text{CO}_2$  in humidified air for 24 h. The amount of E-MEM + 10%FBS was set at the sample surface area to the solution rate as 3  $\text{cm}^2/\text{mL}$ . After immersion, the supernatants were collected and diluted appropriately with E-MEM + 10%FBS. L929 were

seeded on a 24-well microplate at a concentration of 50 cells per well in 0.5 mL of E-MEM + 10%FBS. After 4 h in a CO<sub>2</sub> incubator, the E-MEM + 10%FBS in the wells was discarded and replaced with 0.5 mL of the extract or its dilution. A 0.5 mL portion of E-MEM + 10%FBS was poured into the control wells. Then, the cells were incubated in a CO<sub>2</sub> incubator for 7 d. The colonies formed on the well were fixed and stained to count the number of colonies formed on the bottom of the each well. RPE was calculated by the following equation:

$$\text{RPE}(\%) = (N_{\text{sample}}/N_{\text{control}}) \times 100$$

The bottom areas of the sample and a control well were the same as 1.9 cm<sup>2</sup>. Experiments were carried out in triplicate.

#### 2.4. Surface Characterization

Surface properties were investigated through water contact angle (WCA) and surface roughness. The static water contact angle of a sample surface was measured by a contact angle meter (DM700, Kyowa Interface Science Co. Ltd., Saitama, Japan) under atmospheric conditions at ambient temperature. A distilled water droplet of about 1.5 µL was released onto the surface and the water contact angle at both sides of the droplet was analyzed based on its image using the tangent method after 2 s of waiting time. Sample surface roughness was measured by a confocal laser microscope (VK-9710, Keyence Corp., Osaka, Japan) with the scanning area of 704 × 527. For both WCA and surface roughness, three individual measurements were performed for each type of sample.

#### 2.5. Statistical Analysis

The results are presented as means ± standard deviation. Responses of the cells to the samples were statistically analyzed using the Student's *t*-test. In all cases, *p* values lower than 0.05 were considered statistically significant. Significant changes induced by samples are marked by asterisks in the figures.

### 3. Results

#### 3.1. Microstructure and Mechanical Characterization

The ECAP procedure altered the mechanical properties of SS316L, most notably during the hardness test. The average value of hardness for before ECAP (BE), 120° and 126° was 345 ± 9, 440 ± 16 and 444 ± 19 HV, respectively, suggesting the increase of hardness values ca. 28% by the ECAP processing. Figure 3 illustrates the variation of the hardness values across the sample for three different ECAP conditions. The hardness standard deviation for 120° ECAP was 16 HV, whereas the standard deviation for 126° ECAP was 19 HV indicating the difference in the variation across the radial. The difference in the hardness profile is due to the strain inhomogeneity produced during the ECAP process. Thus, increasing the die angle could result in a reduction in the magnitude of the strain induced as evidence by the average hardness, but the strain induced was more homogeneous throughout the samples.

The microstructure of SS316L before and after ECAP is depicted in Figure 4. The coarse, equiaxed grain was observed in the BE sample as a mean grain size of 11.43 µm. For both ECAP-ed findings, a finer grain with an elongated shape was noted with some sub-grains with mean grain size of 5.95 µm for 120° and 7.10 µm for 126°. Sub-grain formation was also observed in the ECAPed samples. However, the grain refinement was inhomogeneous due to uneven stress distribution after 1-pass ECAP.

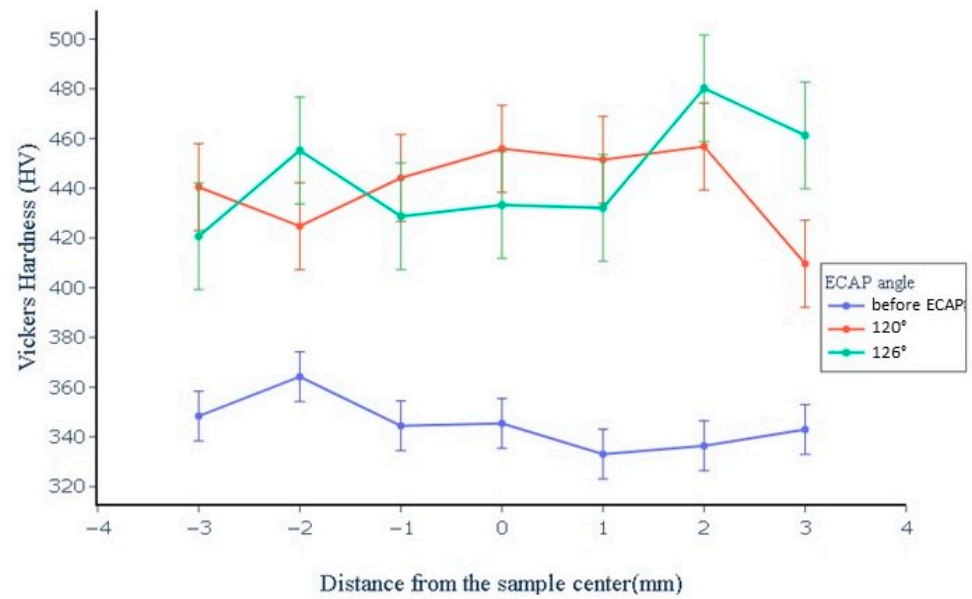


Figure 3. Hardness profile of SS316L samples.

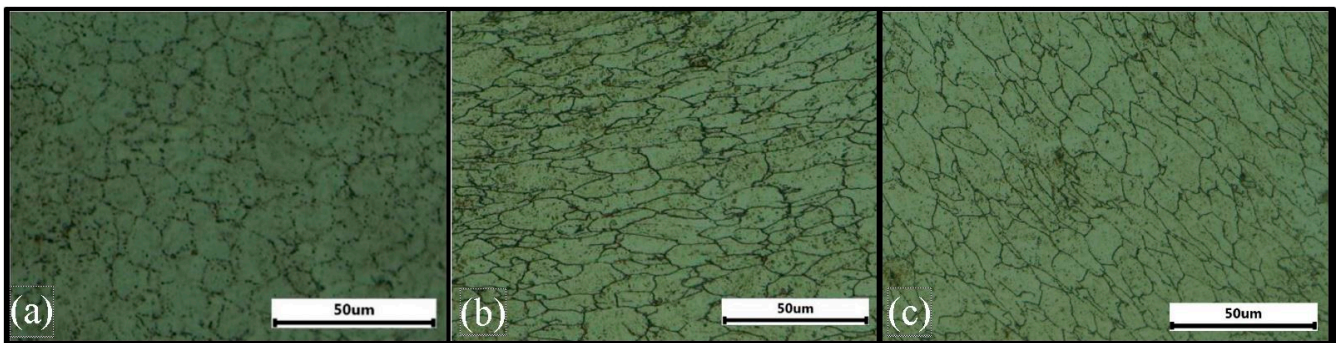


Figure 4. Metallographic observation of SS316L (a) before ECAP, (b) 120° ECAP and (c) 126° ECAP.

### 3.2. Electrochemical Characterization

Typical electrochemical test results of as received and ECAPed SS316L in 0.9% NaCl and E-MEM + 10% NCS are shown in Figure 5a,b, respectively. Corrosion potential ( $E_{corr}$ ), corrosion current densities ( $I_{corr}$ ) and pitting potential ( $E_{pit}$ ) obtained from the polarization curves are listed in Table 1.

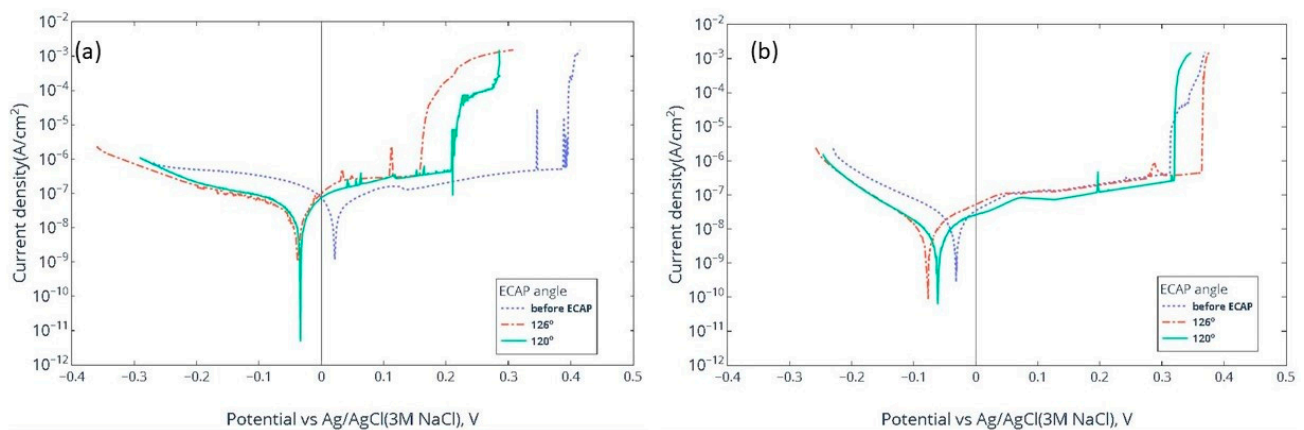


Figure 5. Comparison of the potentiodynamic polarization curves in (a) 0.9% NaCl and (b) E-MEM + 10% NCS.

**Table 1.** Corrosion parameters of 316L SS before and after ECAP.

ECAP Angles	SS316L in 0.9%NaCl			SS316L in E-MEM + 10%NCS		
	$E_{corr}$ (mV)	$I_{corr}$ (nA/cm <sup>2</sup> )	$E_{pit}$ (mV)	$E_{corr}$ (mV)	$I_{corr}$ (nA/cm <sup>2</sup> )	$E_{pit}$ (mV)
BE	3.5 ± 31.1	146.8 ± 100.3	337.0 ± 35.0	−31.5 ± 43.3	126.7 ± 92.4	311.0 ± 99.0
120°	−52.2 ± 49.3	24.6 ± 4.9	205.0 ± 90.0	−59.4 ± 22.0	37.6 ± 24.3	348.0 ± 16.0
126°	−17.9 ± 11.0	107.0 ± 82.0	186.0 ± 96.0	−56.0 ± 26.9	56.6 ± 27.2	307.0 ± 74.0

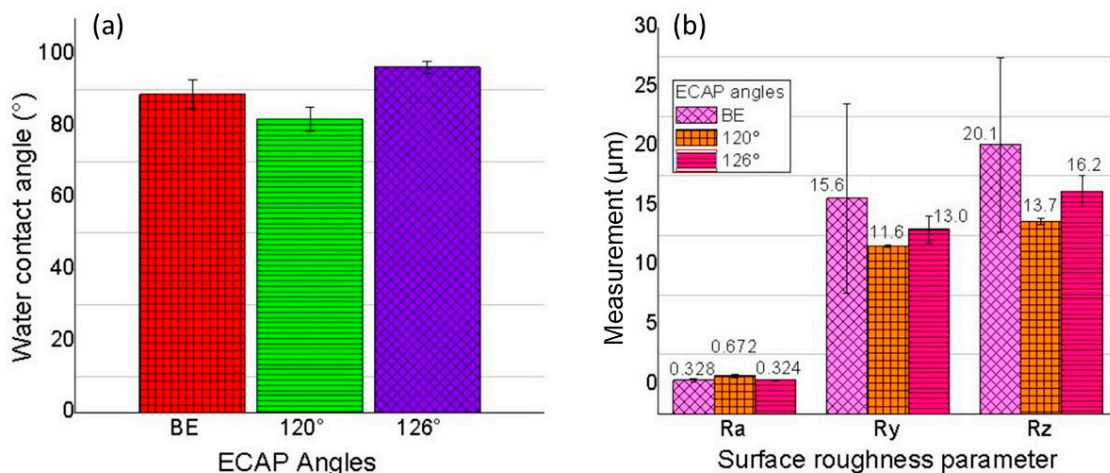
The sample in 0.9% NaCl, before ECAP had the noblest  $E_{corr}$  and  $E_{pit}$  among three samples tested, but the 120° ECAP sample had the smallest  $I_{corr}$ . 120° and 126° ECAP samples showed similar  $E_{corr}$  and  $E_{pit}$ , where both were lower than those of before ECAP sample. However, the  $I_{corr}$  of the 126° ECAP sample was larger than that of the 120° ECAP sample. These facts indicate that the ECAP process influenced the corrosion property of SS316L and that the 120° ECAP sample had slightly better corrosion resistance than the 126° ECAP sample.

In E-MEM + 10% NCS, before ECAP sample had the nobler  $E_{corr}$  but the larger  $I_{corr}$  than ECAP samples, as similar to those in 0.9% NaCl. Concerning the  $E_{pit}$ , 120° ECAP sample was the highest, but the difference was much smaller than those in 0.9% NaCl. The 120° ECAP sample had slightly better  $I_{corr}$  than that of the 126° ECAP sample. These facts indicate that the effect of ECAP on corrosion behavior was much smaller in E-MEM + 10%NCS than that in 0.9% NaCl, and that ECAP at 120° gave a slightly better improvement of corrosion properties than that of ECAP at 126°.

Furthermore, in both solution, ECAP-ed samples had lower  $I_{corr}$  than that of the before ECAP sample, which corresponded to lower anodic kinetic. These PD results suggest that the corrosion resistance of SS316L was improved by ECAP.

### 3.3. Surface Characterization

The wettability of SS316L specimens was investigated using a sessile drop test as shown in Figure 6a. The water contact angle for BE, 120° and 126° samples were  $88.8^\circ \pm 3.9^\circ$ ,  $81.8^\circ \pm 3.3^\circ$  and  $96.3^\circ \pm 1.6^\circ$  respectively with no significant difference were observed between all samples.

**Figure 6.** (a) Contact angle and (b) surface roughness properties of SS316L before and after ECAP.

The major surface roughness parameters of SS316L samples are shown in Figure 6b. For SS316L, the highest value of average roughness ( $R_a$ ) was observed for the 120° ECAP sample, which was almost double of those for BE and 126° ECAP. For the maximum roughness  $R_y$ , the highest value was observed for BE samples followed by 126° and 120°. The same trend was observed in the mean peak-to-valley height ( $R_z$ ) value. However, the

surface roughness parameters also did not have any significant difference among samples. This may be due to all samples being subjected to the same sample preparation prior to testing.

### 3.4. Cytotoxicity Test

The cytotoxicity test results by the direct and the extract method are shown in Figures 7 and 8 respectively. For the direct methods, BE had the highest RPE, followed by 120 and then 126, but no significant difference was observed between the three SS316L samples and control. For the extract methods, BE had an RPE of about 100% for all the extract concentrations, suggesting a similar cellular growth level to the control. For ECAP samples, no sample showed an RPE smaller than 100%, indicating that the extracts of the samples did not have a cytotoxic effect on L929 cells. Furthermore, the value of RPE gradually increased as the extract concentration increases, suggesting the supporting effect of the extracts for L929 growth.

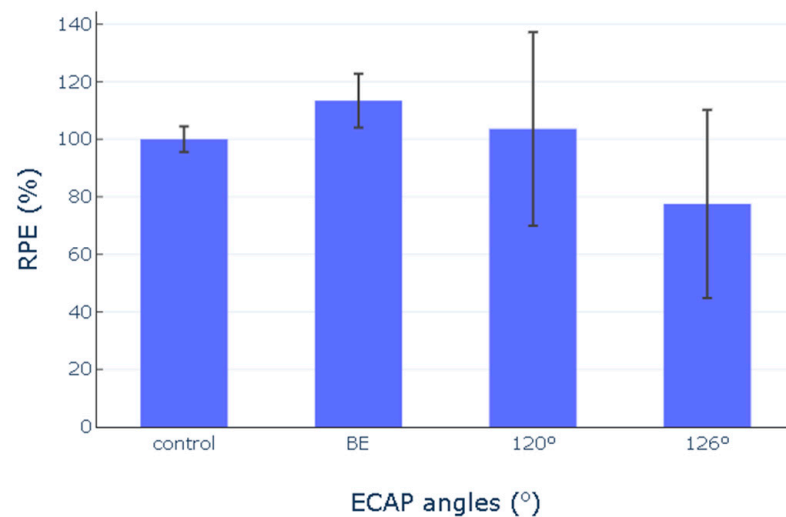


**Figure 7.** Cytotoxicity evaluation of BE and ECAPed SS316L by the direct contact method (mean  $\pm$  sd). No significant difference was observed between the control and three different samples.

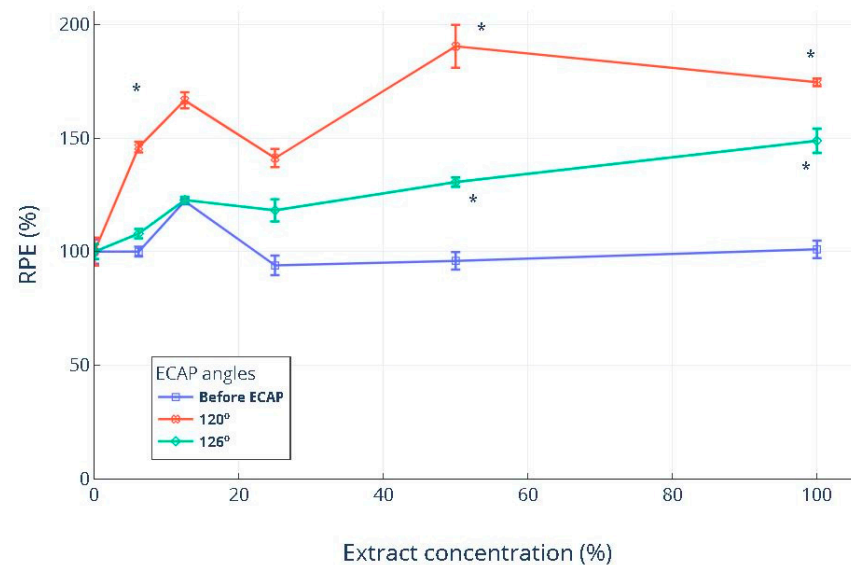


**Figure 8.** Cytotoxicity of SS316L samples evaluated by extract method (mean  $\pm$  sd). \*  $p < 0.05$  to control samples.

#### 4. Discussion

Grain refinement induced by ECAP process is influenced by the die angle used during the experiment. The die angle is the most critical processing parameter in the ECAP process because it affects the total strain imposed on the billet during each pass, thereby affecting the grain refinement of the billet. Additionally, as the number of passes increases, the strain increases. The total strain can be calculated by using the following equation [21]:

$$\varepsilon_{eq} = \frac{1}{\sqrt{3}} \left[ 2\cot\left(\frac{\phi}{2} + \frac{\psi}{2}\right) + \psi \csc\left(\frac{\phi}{2} + \frac{\psi}{2}\right) \right]$$

where  $\phi$  is the internal angle and  $\psi$  is the external angle of the channel of the die. The die channel angle and channel displacement have a significant effect on the magnitude of effective strain in the ECAP with parallel channels process [22]. By decreasing the angle and displacement of the die channel, a greater magnitude of effective strain is imposed on the sample. In general, the die channel angle has a greater effect on the magnitude of an effective strain than on its homogeneity; decreasing the die channel angle results in a greater magnitude of the effective strain imposed on the sample and a requirement of a greater pressing force. However, a channel displacement has a greater effect on the homogeneity of the effective strain; increasing the displacement of the die channel results in a more homogeneous effective strain across the sample cross-section.

It has been reported that stainless steels with an ultrafine grain structure exhibit significantly greater oxidation resistance than their coarse grain counterparts with the same chemical composition [23]. This is due to increased Cr diffusion and the ease with which a compact Cr-oxide layer forms in ultrafine-grained steels. It was observed that the passive film is more stable, compact, and has a lower defect density even though the Cr content in the passive film is higher than the bulk Cr content. The changes in the electrochemical properties of the ultrafine-grained stainless steel may be attributed to the compactness and stability of the passive film [24]. Severe plastic deformation processes have been shown to improve alloy corrosion properties. On the surface of ultrafine grain alloy, a more rapid formation of a passivating layer with improved barrier properties was observed, resulting in improved corrosion resistance of the alloy following severe plastic deformation. Increased grain contact area in the refined microstructure accelerated the formation of a less defective protective barrier surface layer and promoted alloy surface passivation under simulated physiological conditions [25,26]. Electrochemical tests done in this study shows that ECAP influences the corrosion properties of SS316L.  $I_{corr}$  is reduced by ECAP in both conditions tested; 120° ECAP improves better than 126° ECAP.

The ultrafine grain structure also influences the surface topography of the SS316L. The ECAP process at 120° is shown to have the highest mean average surface roughness. Not only that, the surface wettability (WCA) in 120° ECAP also has changed. The reason for this change in wettability may be the enhancement of capillarity resulting from a high number of grain boundaries of ultrafine grain SS316L after conducting ECAP [27]. Surface wettability is a property of the surface energy of ultrafine grain alloys that is strongly related to the grain boundary extension. Energy-dense surfaces exhibit high wettability because the solid–liquid interface reduces the energy [28]. Higher wettability of the nanostructured material may also affect the absorption of proteins hence improved cell proliferation [29].

The improvement in electrochemical and surface properties of ECAP sample has been translated to cytotoxicity test results. By the extract methods, the increase in RPE value showing that the cell proliferation has improved in the ECAP samples compared to BE. This order of the increase in RPE agrees with the order of smaller  $I_{corr}$  in the cell culture medium observed by electrochemical tests. The ECAP process decreases the grain size of the SS316L thus allowing for the formation of a better protective passive film. Even though the ECAP process itself does not change the thickness or composition of the passive film, it has been shown that the passive film formed is more compact and stable leading to better corrosion resistance and suppression of metal ion release [24].



## 5. Conclusions

In this study, ultrafine grain 316L with increased hardness was produced using ECAP at two different die angles of 120° and 126°. Findings showed an improvement in corrosion behaviour of ECAP-ed samples in 0.9% NaCl and E-MEM + 10% NCS. The evaluation of cytotoxicity of ECAPed SS316L also shows improvement compared to BE samples. However, there are no significant changes in wettability and surface roughness on studied samples. Higher strain induced at a lower angle of 120° leads to smaller grain size, higher hardness, better corrosion resistance and better cell proliferation.

**Author Contributions:** Conceptualization, D.N.A.S. and Z.S.Z.; methodology, Z.S.Z. and A.Y.; software, Z.S.Z.; validation, D.N.A.S., Z.S.Z. and A.Y.; formal analysis, D.N.A.S., Z.S.Z. and A.Y.; investigation, Z.S.Z. and A.Y.; resources, D.N.A.S. and A.Y.; data curation, D.N.A.S. and Z.S.Z.; writing—original draft preparation, D.N.A.S., Z.S.Z. and A.Y.; writing—review and editing, D.N.A.S. and A.Y.; visualization, Z.S.Z.; supervision, D.N.A.S.; project administration, D.N.A.S.; funding acquisition, D.N.A.S. All authors have read and agreed to the published version of the manuscript.

**Funding:** This research was funded by Fundamental Research Grant Scheme, Ministry of Higher Education, Malaysia (FRGS/1/2018/TK05/UMP/03/1).

**Institutional Review Board Statement:** Not applicable.

**Informed Consent Statement:** Not applicable.

**Data Availability Statement:** The data presented in this study is available on request from the corresponding author.

**Acknowledgments:** This paper was fully supported by facilities and resources from Universiti Malaysia Pahang and NIMS. The authors would like to acknowledge the support of grants from Fundamental Research Grant Scheme, Ministry of Higher Education, Malaysia: FRGS/1/2018/TK05/UMP/03/1, Masters Research Scheme and PGRS1903162. The authors also would appreciate the support from NIMS as NIMS Internship Program and Project research fund.

**Conflicts of Interest:** The authors declare no conflict of interest.

## References

- Faraji, G.; Mashhadi, M.M.; Kim, H.S. Tubular Channel Angular Pressing (TCAP) as a novel severe plastic deformation method for cylindrical tubes. *Mater. Lett.* **2011**, *65*, 3009–3012. [[CrossRef](#)]
- Shahbaz, M.; Pardis, N.; Ebrahimi, R.; Talebanpour, B. A novel single pass severe plastic deformation technique: Vortex extrusion. *Mater. Sci. Eng. A* **2011**, *530*, 469–472. [[CrossRef](#)]
- Zhou, W.; Yu, J.; Lin, J.; Dean, T.A. Manufacturing a curved profile with fine grains and high strength by differential velocity sideways extrusion. *Int. J. Mach. Tools Manuf.* **2019**, *140*, 77–88. [[CrossRef](#)]
- Zhou, W.; Yu, J.; Lu, X.; Lin, J.; Dean, T.A. A comparative study on deformation mechanisms, microstructures and mechanical properties of wide thin-ribbed sections formed by sideways and forward extrusion. *Int. J. Mach. Tools Manuf.* **2021**, *168*, 103771. [[CrossRef](#)]
- Segal, V. Equal channel angular extrusion: From macromechanics to structure formation. *Mater. Sci. Eng. A* **1999**, *271*, 322–333. [[CrossRef](#)]
- Ferrasse, S.; Segal, V.; Alford, F.; Kardokus, J.; Strothers, S. Scale up and application of equal-channel angular extrusion for the electronics and aerospace industries. *Mater. Sci. Eng. A* **2008**, *493*, 130–140. [[CrossRef](#)]
- Valiev, R. The new trends in fabrication of bulk nanostructured materials by SPD processing. *J. Mater. Sci.* **2007**, *42*, 1483–1490. [[CrossRef](#)]
- Valiev, R.Z.; Estrin, Y.; Horita, Z.; Langdon, T.G.; Zehetbauer, M.J.; Zhu, Y. Producing bulk ultrafine-grained materials by severe plastic deformation: Ten years later. *JOM* **2016**, *68*, 1216–1226. [[CrossRef](#)]
- Valiev, R.Z.; Islamgaliev, R.K.; Alexandrov, I.V. Bulk Nanostructured Materials from Severe Plastic Deformation. *Prog. Mater. Sci.* **2000**, *45*, 103–189. [[CrossRef](#)]
- Srinivas, B.; Srinivasu, C.; Mahesh, B.; Aqheel, M. A review on severe plastic deformation. *Adv. Mater. Manuf. Charact.* **2013**, *3*, 291–295. [[CrossRef](#)]
- Zahari, Z.; Sh'ri, D.A.; Hassan, M.A.; Harun, W.W. In effect of ECAP die angle to the microstructure and mechanical properties of bulk nanostructured Al-6061. In Proceedings of the IOP Conference Series: Materials Science and Engineering, Pekan, Malaysia, 19–21 January 2021; IOP Publishing: Bristol, UK, 2021; p. 012054.
- Shan, Z.; Yang, J.; Fan, J.; Zhang, H.; Zhang, Q.; Wu, Y.; Li, W.; Dong, H.; Xu, B. Extraordinary mechanical properties of AZ61 alloy processed by ECAP with 160° channel angle and EPT. *J. Magnes. Alloy.* **2021**, *9*, 548–559. [[CrossRef](#)]

13. Sordi, V.L.; Mendes Filho, A.A.; Valio, G.T.; Springer, P.; Rubert, J.B.; Ferrante, M. Equal-channel angular pressing: Influence of die design on pressure forces, strain homogeneity, and corner gap formation. *J. Mater. Sci.* **2016**, *51*, 2380–2393. [[CrossRef](#)]
14. Sh'ri, D.A.; Hassan, M.A.; Zahari, Z.; Harun, W.W. Finite element simulation of equal channel angular pressing: Effect of die angle and number of passes. *Int. J. Automot. Mech. Eng.* **2019**, *16*, 6402–6414. [[CrossRef](#)]
15. Alateyah, A.; Ahmed, M.M.; Zedan, Y.; El-Hafez, H.A.; Alawad, M.O.; El-Garaihy, W. Experimental and numerical investigation of the ECAP processed copper: Microstructural evolution, crystallographic texture and hardness homogeneity. *Metals* **2021**, *11*, 607. [[CrossRef](#)]
16. Salleh, M.; Ishak, N.; Yahaya, S.; Abdullah, A. Effect of equal channel angular pressing on the microstructure and mechanical properties of A356 alloy. *J. Adv. Manuf. Technol.* **2018**, *12*, 79–92.
17. Hossain, U.; Ghouse, S.; Nai, K.; Jeffers, J. In additively manufactured Ti6Al4V and SS316L stochastic structures with improved stiffness isotropy for biomaterial applications. In Proceedings of the Orthopaedic Proceedings, Online, 7–8 September 2020; The British Editorial Society of Bone & Joint Surgery: London, UK, 2021; p. 7.
18. Yamamoto, A.; Kohyama, Y.; Kuroda, D.; Hanawa, T. Cytocompatibility evaluation of Ni-free stainless steel manufactured by nitrogen adsorption treatment. *Mater. Sci. Eng. C* **2004**, *24*, 737–743. [[CrossRef](#)]
19. Wallinder, I.O.; Lu, J.; Bertling, S.; Leygraf, C. Release rates of Chromium and Nickel from 304 and 316 stainless steel during urban atmospheric exposure—A combined field and laboratory study. *Corros. Sci.* **2002**, *44*, 2303–2319. [[CrossRef](#)]
20. Eskandari, M.; Yeganeh, M.; Motamedi, M. Investigation in the corrosion behaviour of bulk nanocrystalline 316L austenitic stainless steel in NaCl solution. *Micro Nano Lett.* **2012**, *7*, 380–383. [[CrossRef](#)]
21. Iwahashi, Y.; Horita, Z.; Nemoto, M.; Wang, J.; Langdon, T.G. Principle of equal-channel angular pressing for the processing of ultra-fine grained materials. *Scr. Mater.* **1996**, *35*. [[CrossRef](#)]
22. Al-Mufadi, F.; Djavanroodi, F. Finite element modeling and mechanical properties of aluminum proceed by equal channel angular pressing process. *Int. J. Mater. Metall. Eng.* **2014**, *8*, 1436–1441. [[CrossRef](#)]
23. Gupta, R.; Birbilis, N. The influence of nanocrystalline structure and processing route on corrosion of stainless steel: A review. *Corros. Sci.* **2015**, *92*, 1–15. [[CrossRef](#)]
24. Zheng, Z.; Gao, Y.; Gui, Y.; Zhu, M. Corrosion behaviour of nanocrystalline 304 stainless steel prepared by equal channel angular pressing. *Corros. Sci.* **2012**, *54*, 60–67. [[CrossRef](#)]
25. Awang Shri, D.N.; Tsuchiya, K.; Yamamoto, A. Effect of high-pressure torsion deformation on surface properties and biocompatibility of Ti-50.9 mol.% Ni alloys. *Biointerphases* **2014**, *9*, 029007. [[CrossRef](#)] [[PubMed](#)]
26. Cvijović-Alagić, I.; Laketić, S.; Bajat, J.; Hohenwarter, A.; Rakin, M. Grain refinement effect on the Ti-45Nb alloy electrochemical behavior in simulated physiological solution. *Surf. Coat. Technol.* **2021**, *423*, 127609. [[CrossRef](#)]
27. Masrouri, M.; Faraji, G.; Pedram, M.S.; Sadrkhah, M. In-vivo study of ultrafine-grained CP-Ti dental implants surface modified by SLActive with excellent wettability. *Int. J. Adhes. Adhes.* **2020**, *102*, 102684. [[CrossRef](#)]
28. Bindu, S.; Sanosh, K.; Smetana, K.; Balakrishnan, A.; Kim, T. An in vivo evaluation of ultra-fine grained titanium implants. *J. Mater. Sci. Technol.* **2009**, *25*, 556.
29. Kloss, F.R.; Steinmüller-Nethl, D.; Stigler, R.G.; Ennemoser, T.; Rasse, M.; Hächl, O. In vivo investigation on connective tissue healing to polished surfaces with different surface wettability. *Clin. Oral Implants Res.* **2011**, *22*, 699–705. [[CrossRef](#)] [[PubMed](#)]